# Low-voltage electrostatic modulation of ion diffusion through layered graphene-based nanoporous membranes

Chi Cheng[1,2], Gengping Jiang[3,4], George Philip Simon[2], Jefferson Zhe Liu[5,6*] and Dan Li[1,2*]

[1]Department of Chemical Engineering, University of Melbourne, VIC 3010, Australia; [2]Department of Materials Science and Engineering and New Horizons Research Centre, Monash University, VIC 3800, Australia; [3]College of Science, Wuhan University of Science and Technology, Wuhan 430081, China; [4]The State Key Laboratory of Refractories and Metallurgy, Hubei Province Key Laboratory of Systems Science on Metallurgical Processing, Wuhan University of Science and Technology, Wuhan 430081, China

[5]Department of Mechanical Engineering, University of Melbourne, VIC 3010, Australia; [6]Department of Mechanical and Aerospace Engineering, Monash University, VIC 3800, Australia

Corresponding author Email: dan.li1@unimelb.edu.au (D.L.); zhe.liu@unimelb.edu.au (J.Z.L.)

**Ion transport in nanoconfinement differs from that in bulk, has been extensively researched across scientific and engineering disciplines[1, 2, 3, 4]. For many energy and water applications of nanoporous materials, concentration-driven ion diffusion is simultaneously subjected to a local electric field arising from surface charge or an externally applied potential. Due to the uniquely crowded intermolecular forces under severe nanoconfinement (< 2 nm), the transport behaviours of ions can be influenced by the interfacial electrical double layer (EDL) induced by a surface potential, with complex implications, engendering unusual ion dynamics[5, 6, 7]. However, it remains an experimental challenge to investigate how such a surface potential and its coupling with nanoconfinement manipulate ion diffusion. Here, we exploit the tuneable**

**nanoconfinement in layered graphene-based nanoporous membranes, to show that sub-2 nm confined ion diffusion can be strongly modulated by the surface potential induced EDL. Depending on the potential sign, the combination and concentration of ion pairs, diffusion rates can be reversibly modulated and anomalously enhanced by 4~7 times within 0.5 volts, across a salt concentration gradient up to seawater salinity. Modelling suggests that this anomalously enhanced diffusion be related to the strong ion-ion correlations under severe nanoconfinement, and cannot be explained by conventional theoretical predictions.**

The recent development in two-dimensional (2D) nanofluidics[8, 9], featuring graphene, graphene-based and other atomically thin materials, has enabled severe nanoconfinement tuneable down to subnanometer level to be produced, giving rise to a plethora of anomalous transport phenomena such as ultrafast and precise molecular selectivity[10, 11, 12]. We have previously shown that by the supramolecular assembly of chemically converted graphene, a layered, nanoporous gel membrane (Fig. 1a) can be readily produced, containing a continuous cascading nanochannel network[13]. The average interlayer spacing, $d$, of the membranes can be tuned in the range of a few to sub-nanometres[14]. Under such a severe nanoconfinement (< 2 nm), it should contain almost entirely an interfacial electrical double layer (EDL) without bulk solution between any two graphene layers, even if the salt concentration is up to 0.1 M. Furthermore, electrically conducting graphene materials can act simultaneously as a channel wall and a gate electrode. This allows for effective modulation of the interfacial EDL electrostatically *in-situ*, without the need for an additional dielectric layer of a channel wall made with, for example, silicon-based materials as used in conventional devices such as field-effect nanofluidic transistors[15]. Due to the exceptionally large EDL capacitance of chemically converted graphene[16], a significant change to the interfacial double

layer ion population and distribution can be readily achieved by applying a very low surface potential (< 1 V). Additionally, since the membrane is a multi-channel platform, a much higher flux is possible compared to single channel devices, allowing ready detection of permeate signals within a time scale of a few minutes[14]. This means that layered graphene-based nanoporous membranes represent a unique experimental platform upon which ion diffusion through a barrier of nanoconfined EDL can be studied.

We used the experiment setup shown in Fig. 1a to examine how concentration-driven ion diffusion is influenced by the EDL induced by varying the surface potential in a confined nanochannel using the layered graphene-based nanoporous membrane. Since the membrane is both mechanically self-supporting and electrically conductive, a gate potential ($V_g$) was applied directly to the membrane to tune the EDL enclosed between the layers of graphene materials. A concentration gradient was then created to drive ions to diffuse through the series of cascading graphene nanochannels in the membranes with the interlayer spacing varied from 5.4 nm to 0.8 nm (Supplementary Fig. 1). Such a design allows for the study of ion diffusion, recorded as diffusion flux (*J*), through nanoconfined EDL,whose structure can be tuned *in-situ* by an externally applied potential or the degree of nanoconfinement (i.e. the interlayer spacing).

Figure 1b shows the diffusion of KCl through the layered graphene membrane under a constant $V_g$, whereby the diffusion rates were significantly changed with different $V_g$. Specifically, as the $V_g$ was changed from –0.2 V to –0.5 V, diffusion fluxes were enhanced by approximately four times from $7.93\times10^{-3}$ to $3.02\times10^{-2}$ mol $h^{-1}$ $m^{-2}$. By contrast, only a slight flux enhancement was observed when the membrane was positively charged up to 0.5 V (Supplementary Fig. 2a). This asymmetry between $K^+$ and $Cl^-$ is not uncommon under

82 nanoconfinement, although they exhibit the same diffusion coefficient and mobilities in bulk
83 solutions. Due to the different water polarisation around cations and anions, $K^+$ gives higher
84 EDL capacitance than $Cl^-$ on graphene surface[17]. As such, the channel ion populations
85 experience an asymmetric rearrangement as the charging status of the membrane shifts from
86 positive to negative polarisation. Flux responses to immediate changes in the $V_g$ were further
87 investigated and the results are shown in Fig. 1c. Ion permeation rates across the layered
88 graphene membrane were spontaneously changed, depending on the $V_g$ applied, as seen by
89 the sharp gradient change of the diffusion curves. Cycling of the $V_g$ between –0.5 V and 0.2
90 V, and subsequent comparison of fluxes measured at each voltage showed that such an
91 electrostatic modulation effect of ion transport through the membrane was reversible (Fig.
92 1d). The flux change during one $V_g$ shift was completed within a timescale of tens of
93 seconds. We further confirmed that the enhancement of $J$ with increasing $V_g$ was mainly
94 resulted from the change of the graphene-enclosed EDL structure by ruling out the influence
95 from membrane expansion (Supplementary Figs. 2b and c) and water oxidation/reduction
96 (Supplementary Fig. 3) during the diffusion tests. Ion concentrations in the permeate
97 compartment at the end of diffusion tests were also independently analysed using inductively
98 coupled plasma mass spectrometry. The results are in good agreement with those derived
99 from the solution conductivity analysis (Supplementary Fig. 4).
100
101 The critical role of severe nanoconfinement is shown by displaying the full $J$ – $V_g$
102 relationships in which the ion fluxes at different $V_g$ were normalised to that of $V_g = 0$ V (Figs.
103 2a-c). The curve profile was asymmetrically parabolic, with a sharp increase in flux values as
104 the $V_g$ became more negative to –0.5 V, and through membranes with $d$ smaller than 2 nm
105 (black and orange curves in Fig. 2a). The normalized ion flux was three times higher through
106 a membrane with $d$ = 0.8 nm than a membrane with $d$ = 5.4 nm, as the $V_g$ was increased from

0 to –0.5 V, and measured for the same feed concentration of 0.1 M. In the cases of greater *d*, the modulation of ion diffusion was reduced. Through a membrane with the largest experimented *d* of 5.4 nm, the enhancement of ion flux diminished, and the flux even exhibited a slight decrease as $V_g$ approached either ± 0.5 V. This is consistent with a recent report that the rate of ion diffusion through a mesoporous carbon membranes with a pore size of ~7.8 nm remained unchanged when a gate potential of up to -0.8 V was applied[18].

Further investigation on the dependence of modulation ratio on concentration gradient (Fig. 2) suggested that the mechanism of such modulated diffusion is closely related to the structural variation of nanoconfined EDL. As the ion concentration in the feed reservoir was increased, and the EDL would be thinner and more compact to the surface, the modulation of ion diffusion was reduced and diminished when the feed concentration reached 0.5 M, even when the channel size is as small as 0.8 nm. In cases where the membrane was positively charged, a slight flux increase was also observed. This asymmetric $J$ – $V_g$ relationship depending on the sign of surface potential applied indicates the essential difference between the EDL structures in which either $K^+$ or $Cl^-$ were the counter ions.

Such enhanced ion diffusion through the EDL induced with increased surface potential under nanoconfinement of less than 2 nm is contrary to the predictions based on the classical ion transport theory[2]. Our simulation study based on the classic Poisson-Nernst-Planck (PNP) model[19], showed that diffusion flux indeed should decrease through the EDL confined in nanochannels with a size of 2 nm with the increase of gate potential (Supplementary Figs. 5 and 6). The results revealed significant co-ion depletion in the overlapping EDL structure confined between the graphene layers, with an increased surface potential (inset in Supplementary Fig. 6). The decreased co-ion concentration in EDL lead to an accumulation

of counter-ions in the drain side and thus a build-up of the Donnan potential. Such an potential, once established, will reduce the counter-ion flux to match the co-ion flux. Further investigations on other possible factors, including the medium dielectric constant (Supplementary Fig. 6), and an increased ion diffusion coefficient (Supplementary Fig. 7), which are known to vary under severe nanoconfinement, also confirmed a prohibited diffusion under increased surface potential, consistent with the Teorell-Meyer-Sievers or space-charge models for nanofiltration membrane[20]. Such a reduced ion flux through the unipolar EDL has indeed previously been used for salt rejection[21], and to control membrane selectivity[22].

Similar anomalous, electrostatically-modulated ion diffusion phenomena under extreme nanoconfinement were also observed with both monovalent and bivalent cation/anion pairs, though the degree of modulated diffusion was ion specific. Among the monovalent and bivalent cation/anion pairs studied, the degree of modulated diffusion through a membrane with *d* of 2 nm was found to reach a factor of over 6 for $K_2SO_4$, nearly double the modulation ratio of KCl within the same $V_g$ ranging from 0 to –0.5 V, while negligible modulation was seen for $MgCl_2$ (Fig. 3a). When $Cl^-$ was selected as the anion and paired with $Li^+$, $Na^+$, $K^+$ and $Cs^+$, respectively, ion diffusion through the layered graphene membranes was enhanced, yet exhibited insignificant ion specificity, and a modulation ratio approaching four under a $V_g$ of –0.5 V, compared with a $V_g$ of –0.2 V (Supplementary Fig. 8). In addition, if alkali cations were paired with molecular anions of weak carboxylic acids, which are commonly present on the surfaces of intra- and extracellular proteins, the modulated diffusion could be observed, even under a feed concentration up to 0.5 M (Fig. 3b). Importantly, the contrast between

155 sodium acetate and sodium chloride indicates the significant role the specific noncovalent
156 interactions between hydrated cations and anions plays in the modulation mechanism.
157
158 To develop a more realistic model to elucidate this unexpected phenomena, we considered the
159 role of the short-range, ion-specific ion-ion correlations in enhancing the ion diffusion under
160 extreme nanoconfinement and a surface potential. Recent developments suggest that the non-
161 Coulombic-form, ion-ion correlations[23] can contribute considerably to the alternation of ion
162 arrangements of the EDL, particularly in the first few ion layers closely confined to the
163 electrode/electrolyte interface. Instead of an ideal, exponential decay of ion concentrations in
164 the EDL from the surface towards the nanochannel centre, an oscillating counter- and co-ion
165 concentration profiles emerge where there can be a peak of much concentrated co-ion layer as
166 a result of such ion-ion correlations. This interaction among counter- and co-ions has become
167 crucial in describing unconventional interfacial phenomenon *e.g.* "overscreening"[24] and
168 "charge inversion"[25]. Considering the extreme nanoconfinement electrolytes experience in a
169 sub-2 nm graphene nanochannel (< 10 layers of water molecules) as in our experiment, it is
170 possible that such ion-ion correlations cannot be completely neglected. We incorporated the
171 ion-ion correlations into the PNP model (later referred to as PNP/IC model), according to
172 Bazant's work[24] (Supplementary Eq. 4-5), and the geometry of the simulation model
173 illustrated in the inset of Fig. 4d.
174
175 Simulation with the effect of ion-ion correlations (PNP/IC) considered showed that the
176 channel concentrations, especially the co-ion concentrations, markedly increased after
177 demonstrating a minimum with a higher surface potential, which was in contrast to what was
178 revealed with the conventional PNP model (hollow symbols in Fig. 4a). Instead of co-ion
179 depletion traditionally expected for electrostatically charged EDL under nanoconfinement,

the PNP/IC model predicted an unexpected increase in co-ion concentration with increasing the surface potential. This would lead to the build-up of Donnan potential being hindered, which was confirmed by experiment (Fig. 4b), resulting in an enhanced ion flux as seen in Figure 4c (solid) for the $J - V_g$ relationship. The trend that weakened diffusion enhancement in channel with larger sizes could also be predicted with the PNP/IC model. Shown in Fig. 4d, as the channel size decreases, an increase in the level of enhanced diffusion is observed. Furthermore, the magnitude of increase in the relative flux with $V_g$ is greater for lower feed concentrations (50 mM) than a higher one (0.5 M), which is also consistent with experimental observations.

Although ion-ion correlations have long been acknowledged in colloidal and electrochemical systems[23, 26], their influence on ion transport properties has been insignificant and often neglected in traditional nanoporous materials systems. Our results suggest that such correlations among ions could play a key role in modulating the ion diffusion behaviours if the nanoconfinement, materials and nanoporous structure are appropriately designed. As an example, choosing $SO_4^{2-}$ as co-ions leads to a more significant degree of modulated diffusion as a result of its stronger ion-ion correlations with cations[27]. Under the nanoconfinement of < 2 nm, a significant drop in the medium dielectric constant (from 78 to 10 for aqueous medium) is expected[28], affording a much stronger effect of ion-ion correlations on diffusion as a weakening shielding from the dielectric medium (Supplementary Fig. 10). Additionally, the large double layer capacitance of the cascading nanoslits in layered graphene membranes enables a strong manipulation of the overlapping EDL structure, and translates its influence on ion diffusion at the nanoscale to an readily observable macroscopic modulation phenomena using a relative low surface potential.

204

205 The ability to effectively modulate the transport of charge carriers in materials by a small
206 external voltage, particularly at the nanoscale, has enabled important technologies such as
207 modern electronics which is largely built on the field effect in semiconducting materials. It
208 has been attempted, as yet with limited success, to extend the use of the electric field to
209 modulate ion transport in nanochannels[29]. Given there are few materials choices currently
210 available for creating extreme nanoconfinement at the molecular level, it has been difficult to
211 determine whether and how the fundamental diffusion of ionic species in liquids can be
212 effectively modulated with a small potential similar to the field effect in solid semiconducting
213 materials. This mechanism of strongly modulated nanoconfined ion diffusion with a low
214 surface potential could enable effective, fast modulation of the diffusion of ionic species
215 within a voltage range compatible with physiological concentrations and environments, such
216 as rapid and selective dialysis and controlled release of ionic drugs. Given the nature of
217 molecular interactions in extreme nanoconfinement coupling with electric fields is complex,
218 the observed modulated ion transport behaviour and the peculiar ion specificity shows
219 promise for researching into the electric field effect in nanoconfined liquid materials, which
220 remains largely unexplored. With the advancement in engineering and scale up production of,
221 atomically-precise nano-pores, -channels and -circuits, field-effect control of ionic transport
222 associated with size reduction is likely to enable logic and signalling machineries and
223 devices, beyond conventional use of nanoionics in energy storage, separation and water
224 desalination.

225

226 **References**

227 1. Bocquet, L., Charlaix, E. Nanofluidics, from bulk to interfaces. *Chem. Soc. Rev.* **39,**
228 1073-1095 (2010).
229

2. Sparreboom, W., van den Berg, A., Eijkel, J. C .T. Principles and applications of nanofluidic transport. *Nat. Nanotechnol.* **4**, 713-720 (2009).

3. Duan, C., Majumdar, A. Anomalous ion transport in 2-nm hydrophilic nanochannels. *Nat. Nanotechnol.* **5**, 848-852 (2010).

4. Maier, J. Nanoionics: ion transport and electrochemical storage in confined systems. *Nat. Mater.* **4**, 805-815 (2005).

5. Feng, J. et al. Observation of ionic Coulomb blockade in nanopores. *Nat. Mater.* **15,** 850-855 (2016).

6. Griffin, J. M. et al. In situ NMR and electrochemical quartz crystal microbalance techniques reveal the structure of the electrical double layer in supercapacitors. *Nat. Mater.* **14**, 812-819 (2015).

7. Kondrat, S., Wu, P., Qiao, R., Kornyshev, A. A. Accelerating charging dynamics in subnanometre pores. *Nat. Mater.* **13**, 387-393 (2014).

8. Koltonow, A. R., Huang, J. Two-dimensional nanofluidics. *Science* **351**, 1395-1396 (2016).

9. Gao, J., Feng, Y., Guo, W., Jiang, L. Nanofluidics in two-dimensional layered materials: inspirations from nature. *Chem. Soc. Rev.* **46**, 5400-5424 (2017).

10. Joshi, R. K. et al. Precise and Ultrafast Molecular Sieving Through Graphene Oxide Membranes. *Science* **343**, 752-754 (2014).

11. Morelos-Gomez, A. et al. Effective NaCl and dye rejection of hybrid graphene oxide/graphene layered membranes. *Nat. Nanotechnol.* **12,** 1083-1088 (2017)

12. Chen, L. et al. Ion sieving in graphene oxide membranes via cationic control of interlayer spacing. *Nature* **550 ,** 380-383 (2017).

13. Yang, X. et al. Ordered Gelation of Chemically Converted Graphene for Next-Generation Electroconductive Hydrogel Films. *Angew. Chem. In. Ed.* **50**, 7325-7328 (2011).

14. Cheng, C. et al. Ion transport in complex layered graphene-based membranes with tuneable interlayer spacing. *Sci. Adv.* **2,** e1501272 (2016).

15. Karnik, R. et al. Electrostatic Control of Ions and Molecules in Nanofluidic Transistors. *Nano Lett.* **5**, 943-948 (2005).

16. Yang, X., Cheng, C., Wang, Y., Qiu, L., Li, D. Liquid-Mediated Dense Integration of Graphene Materials for Compact Capacitive Energy Storage. *Science* **341**, 534-537 (2013).

17. Jiang, G., Cheng, C., Li, D., Liu, J. Z. Molecular dynamics simulations of the electric double layer capacitance of graphene electrodes in mono-valent aqueous electrolytes. *Nano Res.* **9**, 174-186 (2016).

18. Surwade, S. P. et al. Electrochemical Control of Ion Transport through a Mesoporous Carbon Membrane. *Langmuir* **30**, 3606-3611 (2014).

19. Borukhov, I., Andelman, D., Orland, H. Steric Effects in Electrolytes: A Modified Poisson-Boltzmann Equation. *Phys. Rev. Lett.* **79**, 435-438 (1997).

20. Schaefer, A., Fane, A. G., Waite, T. *Nanofiltration: Principles and Applications 2nd Ed.* (2017).

21. Tsuru, T., Nakao, S. I., Kimura, S. Calculation of Ion Rejection by Extended Nernst–Planck Equation with Charged Reverse Osmosis Membranes for Single and Mixed Electrolyte Solutions. *J. Chem. Eng. JP* **24**, 511-517 (1991).

22. Nishizawa, M., Menon, V. P., Martin, C. R. Metal Nanotubule Membranes with Electrochemically Switchable Ion-Transport Selectivity. *Science* **268**, 700-702 (1995).

23. Yan, L. Electrostatic correlations: from plasma to biology. *Rep. Progr. Phys.* **65**, 1577 (2002).

24. Bazant, M. Z., Storey, B. D., Kornyshev, A. A. Double layer in ionic liquids: overscreening versus crowding. *Phys. Rev. Lett.* **106,** 046102 (2011).

25. Grosberg, A. Y., Nguyen, T., Shklovskii, B. Colloquium: the physics of charge inversion in chemical and biological systems. *Rev. moder. phys.* **74**, 329 (2002).

26. Quesada-Pérez, M., González-Tovar, E., Martín-Molina, A., Lozada-Cassou, M., Hidalgo-Álvarez, R. Overcharging in colloids: beyond the poisson–boltzmann approach. *ChemPhysChem* **4**, 234-248 (2003).

27. van der Vegt, N. F. A. et al. Water-Mediated Ion Pairing: Occurrence and Relevance. *Chem. Rev.* **116**, 7626-7641 (2016).

28. Ballenegger, V., Hansen, J. P. Dielectric permittivity profiles of confined polar fluids. *J. Chem. Phys.* **122,** 114711 (2005).

29. Prakash, S., Conlisk, A. T. Field effect nanofluidics. *Lab Chip* **16**, 3855-3865 (2016).

**Acknowledgements**

We would like to acknowledge the financial support from the Australia Research Council. This work made use of the facilities at the Monash Centre for Electron Microscopy (MCEM).

**Author contribution statement**

C.C. conceived, designed, carried out the experiments under the guidance of D.L. and G.P.S. D.L. and C.C. formulated the concept of using nano-confined electrical double layer for ion modulation. G.J. designed and carried out the theoretical modelling under the guidance of J.Z.L. All authors discussed and interpreted the results. C.C. and G.J. wrote the manuscript with contributions from all the other authors.

**Competing interests**

The authors declare no competing interests

**Figure captions**

**Fig. 1: Ion diffusion through nanoconfined EDLs in charged layered graphene-based nanoporous membranes. a,** Schematic showing the experiment step-up for the investigation of ion diffusion (0.05 M KCl) through nanoconfined EDLs in charged, layered graphene-based nanoporous membranes with a $d$ = 2 nm. Under such severe nanoconfinement, the electrical double layer, highlighted in bright red and yellow colours, fully fills the membrane. Potentials versus a Ag/AgCl reference electrode (RE) were applied directly to the membrane, which acted as the working electrode (WE). Together with a platinum mesh counter electrode (CE), the feed reservoir is essentially a standard three-terminal electrochemical cell. Inset is an optical image of the membrane material. **b,** Steady-state diffusion curves obtained under varied $V_g$ from –0.5, –0.4 to –0.2 V. **c,** Steady-state diffusion curves obtained under a programmed $V_g$ sequence from –0.2, –0.4, –0.5, 0, 0.2, 0.4 to 0.5 V. The voltage changed immediately after each potential step and was held for 90 minutes. The diffusion curves are shown as the grey line, upon which linear regression was carried out for each $V_g$ and shown as blue lines. Data were used after 70 minutes to allow diffusion to reach to the steady state. **d**, Reversible modulation of ion diffusion with a $V_g$ whose values were varied between –0.5 V and 0.2 V for multiple cycles. Inset (up) shows the membrane flux measured under 4 cycles of alternating $V_g$ over the course of 10 hours. Inset (down) is a zoom-in of the flux transition as the $V_g$ changed from –0.5 V to 0.2 V at the second cycle.

**Fig. 2: Normalized membrane flux dependence on $V_g$ under various levels of nanoconfinement and concentration gradient.** Profiles of the modulated ion diffusion

through charged layered graphene-based nanoporous membranes (with a *d* of 2 nm) measured under different feed concentrations from **a,** 0.05 M (black), **b,** 0.1 M (black) to **c,** 0.5 M(black); and the profile dependence on nanoconfinement achieved via varying the membrane interlayer spacing from 0.8 nm (yellow), 2.0 nm (black) to 5.4 nm (green). Ion fluxes under various charging conditions were normalized to that obtained at zero volts vs. Ag/AgCl reference electrode. The electrolyte used was a KCl aqueous solution. The average of three independent tests are plotted in the figures.

**Fig. 3: Ion specific electrostatically modulated ion diffusion through layered graphene-based nanoporous membranes (*d* = 2 nm). a,** Profiles of normalised membrane flux dependence on $V_g$ measured in KCl, $K_2SO_4$, $MgSO_4$ and $MgCl_2$ electrolytes and with a feed concentration of 50 mM. The average of three independent tests are plotted in the figures. **b,** Steady-state diffusion curves of sodium acetate (black), KCl (purple) and NaCl (blue) with a feed concentration of 0.5 M under a $V_g$ sequence from –0.5 to 0.5 V. The diffusion curves were shown as the grey dot lines, upon which linear regression was carried out for each $V_g$.

**Fig. 4: Role of ion-ion correlations in altering channel counter- and co-ion concentrations, membrane potential and membrane flux against varied channel height. a,** the figure shows the normalized concentrations of both co- and counter-ion (inset) in an array of 2-nm graphene cascading nanoslits simulated with (solid) and without (open) ion-ion correlations contribution under various $V_g$. Feed concentrations were varied from 0.05 M to 0.5 M. **b,** Membrane potential measured by experiment during steady-state, voltage-modulated diffusion against a varied $V_g$. The concentration gradient was created with a feed solution of 0.1 M, and a permeate solution of 1 mM KCl. Inset shows the membrane potential obtained from continuum simulation based on PNP model (empty purple circles) and PNP/IC model (filled purple circles). **c,** the figure shows the corresponding $J - V_g$ relationships in 2-nm graphene nanoslits. **d,** the figure shows the effect of channel size on flux enhancement simulated with $V_g = -0.3$ V and a feed concentration of 0.05 M. The inset shows the

cascading graphene nanoslits model geometry used for simulation. Reservoir length ($L_{res}$), nanoslit membrane length ($L_{mem}$), the lateral length of graphene sheet ($L_G$), sheet-to-sheet aperture size ($\delta$) and interlayer spacing ($d$) were 100, 80, 55, 2 and 2 nm respectively. These parameters were adopted from previous work in Ref. [17]. The lower range of the medium dielectric constant ($\epsilon_d$) was set to be 10 inside the graphene nanochannels with a size of 2 nm, and was determined by a separate Molecular Dynamics (MD) simulation (Supplementary Fig. 9). The correlation length ($l_c$) in the PNP/IC model was set to be 0.66 nm which is the size of hydrated $K^+$ and $Cl^-$ ions.

## Methods

*Fabrication of the layered graphene-based nonporous membranes*

The layered graphene-based nanoporous membranes were prepared via direct-flow filtration of chemically converted graphene colloids. Chemically converted graphene (CCG) dispersions were synthesized following the method previously described in Ref.[30]. Briefly, graphene oxide colloid (0.5 mg/ml, 100 ml) prepared with the modified Hummers' method was initially mixed with 0.2 ml hydrazine (35 wt% in water) and 0.35 ml ammonia (28 wt% in water) solution in a glass flask. After being vigorously shaken for a few minutes, the flask was put into a water bath (~100 $^oC$) for 3 hours. A controlled amount of the as-obtained CCG dispersion was vacuum filtrated through a mixed cellulose ester filter membrane (0.05 μm pore size). The vacuum was disconnected immediately after all free CCG dispersion was gone from the filtrate cake, at which a wet gel membrane remained. The gel membrane was then carefully peeled from the filter, immediately transferred to a Petri dish and immersed in deionized water overnight to further remove the remaining ammonia and unreacted hydrazine. To ensure sufficient mechanical robustness and integrity of the freestanding membranes, the CCG mass loading of all wet gel membrane samples was controlled to be 1 $mg/cm^2$ (A schematic of graphene membrane preparation was shown in Supplementary Fig. 1).

*Varying the interlayer spacing of the layered graphene-based nanoporous membranes*

Capillary compression method was used, described in Ref. [16], and shown in the Supplementary Fig.1, to tune the average interlayer spacing of the nanoporous graphene membranes. Briefly, the water inside the as-assembled gel membranes was first exchanged

with a controlled ratio of volatile/non-volatile miscible solution (water/ sulphuric acid solution in this case). The volatile liquid inside the gel membrane was then selectively removed via vacuum evaporation. The removal of the volatile component of the miscible solution exerted capillary compression between CCG layers, leading to a uniform shrinkage of membrane thickness and thereby decreasing the average interlayer spacing in a collective manner. As the non-volatile part of the miscible solution in the gel membrane remained, the average interlayer spacing could be readily tuned by adjusting the ratio of volatile/non-volatile solutions. Subsequently, the as-compressed gel membranes were washed thoroughly with deionized water, exchanging the non-volatile liquid back to water prior to test. It is worthwhile to point out that this exchange of non-volatile back to water step would cause a slightly increased membrane thickness. The average interlayer spacing, *d*, was estimated following the equation:

$$\boldsymbol{d} = \frac{\boldsymbol{Areal\ mass\ density\ of\ graphene} \times \boldsymbol{thickness\ of\ the\ gel\ membranes}}{\boldsymbol{Areal\ mass\ loading\ of\ the\ gel\ membranes}} \quad \text{Eq.1}$$

in which, the thickness of the gel membranes was measured after the final "exchange of liquid" step (Supplementary Fig. 1).

*Measurement of ion diffusion across charged nanoporous graphene membranes*

As-prepared layered graphene-based nanoporous membranes were mounted between two clamp holders (an image shown in the Supplementary Fig. 1), where one side of the membrane was attached to a platinum ring, making the membrane the working electrode in a three-terminal electrochemical cell. Two compartments, namely the feed and permeate, were then connected to each side of the membrane holder, constituting a standard configuration for measuring membrane permeability. The feed compartment was filled with 0.05, 0.1 and 0.5 M electrolyte solutions to be individually tested, while the permeate was filled equivalent volume of deionized water with conductivity less than 4 μS/cm. A constant potential within a range from –0.5 V to 0.5 V was generated using a BioLogic VMP-300 system while the ion permeation through the membranes was constantly monitored by a conductivity meter. Both counter (a platinum mesh) and Ag/AgCl reference electrodes were placed at fixed positions in the feed compartment, close to the membrane surface to minimize Ohmic loss. The conductivity change in the permeate reservoir was plotted against elapsed time to give the

diffusion curve. To ensure the concentration gradient between feed and permeate reservoirs remained constant throughout the diffusion measurement, the conductivity variance of the feed reservoir was monitored before and after the diffusion test. For the lowest feed concentration of 0.05 M, the feed conductivity values before and after the diffusion at the highest membrane potential of -0.5 V were 6.31 μS/cm and 6.21 μS/cm, respectively. The decrease in feed solution concentration was less than 2%. To further ensure that the concentration difference between the feed and permeate reservoirs remained constant throughout the diffusion test, no readings were made after the concentration in the permeate reached $1.4 \times 10^{-4}$ M (~20 μS/cm at room temperature). Solutions in both reservoirs were constantly circulated, to avoid possible concentration gradient build-up at membrane surfaces.

A variety of ions were tested to see if their fluxes through the layered graphene membrane could also be modulated by the applied potential. In order to properly examine and compare the effect of different ion pairs, our choices are mainly focused on simple alkali metal cations including $Li^+$, $Na^+$, $K^+$ and $Cs^+$ then paired with $Cl^-$ and $SO_4^{2-}$, in particular for a known strong ion-ion correlations of $SO_4^{2-}$ with cations[27].

Because of the micro-corrugated molecular configuration of CCG[31], it is difficult to gain meaningful information on the average interlayer spacing of the membrane during diffusion testing[16]. We measured the membrane thickness variation *in-situ* as an indicator for any structural deformation of the membrane during charging. Additionally, the layered nanoporous graphene-based membrane can retain a stable structure under both negatively and positively polarised as revealed by thousands of electrochemical cycling experiments [16].

*Mean-field theory modeling of ion diffusion through charged graphene nanochannels*

To gain further insights into the experimentally observed voltage-modulated ion diffusion phenomenon, we carried out simulations to research into the effect of the interplay among various interactions in nanoconfined fluids. We used a modified Poisson-Nernst-Planck model (described as PNP model in this work) to simulate ion diffusion through charged graphene nanochannels, which took into account the ion steric effect in solutions with high concentrations of ~ 1 M and under high potentials ($\phi \gg \frac{k_B T}{ze}$)[19, 32]. The solution for a binary

475 symmetric electrolyte *e.g.* KCl, whose cation and anion were of nearly the same size was
476 presented as follows,

$$\epsilon_0 \epsilon \nabla^2 \phi = -\rho = -\sum_{i=i}^{N} z_i e N_A n_i \qquad \text{Eq.2}$$

$$\frac{\partial n_i}{\partial t} = D_i \nabla^2 n_i + e z_i \mu_i n_i \nabla \phi + \frac{D_i N_A a^3 n_i \nabla (n_+ + n_-)}{1 - N_A a^3 (n_+ + n_-)} \qquad \text{Eq.3}$$

477 where $a$ = 0.66 nm, the size of both cation and anion of KCl aqueous electrolyte; $\epsilon_0$ and $\epsilon$
478 were the vacuum and relative permittivity of solution; $\phi$ was the electric potential
479 distribution; $\rho$ was the net charge density; $N_A$ was the Avogadro constant; $D_i$, $\mu_i$, $z_i$, $n_i$ were
480 diffusivity, electro-mobility, valence number and concentration distribution for species $i$,
481 respectively. The diffusivity and electro-mobility of $K^+$ and $Cl^-$ ions were considered the
482 same[14]. The last term of Eq.3, also called the entropy term, was added as a correction for
483 finite ion size. This was to ensure that the maximum concentration of ions $(n_+ + n_-)$ in
484 reservoirs did not $n_{max} = 1/N_A a^3$[24].

485 A 40-layer parallel-aligned graphene array shown in the Supplementary Fig. 5 (representing
486 the structure of the graphene membrane used in experiment) was sandwiched in between two
487 100-nm-in-length feed and permeate reservoirs. We adopted the optimized geometries of the
488 graphene array from our previous work in which the three critical parameters are the length
489 of graphene sheet $L_G$ = 55 nm, channel height (interlayer spacing) $d$ = 2 nm and in-plane
490 aperture size $\delta$ = 2 nm[14]. Given the symmetry of the channel array structure, we built and
491 studied only half of the minimal unit cell. An electric potential difference of $V_g$ = 0~0.3 V
492 between $\Gamma_1$ and $\Gamma_G$ was imposed to mimic the gate voltage ($V_g$) applied in the experiment.
493 Impermeable boundary conditions were employed at both the entrance of $\Gamma_1$ and $\Gamma_4$ for ionic
494 concentration and electric field. Feed concentrations in the feed reservoir (0.05, 0.01 to 0.5 M
495 as used in experiments) were fixed at the entrance $\Gamma_1$, and the concentrations of cations (or
496 anions) at the permeate exit $\Gamma_4$ were set as $1\times10^{-5}$ M. To simulate the stationary state of
497 diffusion as reflected by a constant membrane permeability observed in experiment, and the
498 dilute solution in the permeate reservoir, the flux of both cations and anions at the exit $\Gamma_4$
499 were set as equal.

The effect of a possible decrease in dielectric constant arising from strong nanoconfinement[33] was investigated via varying the dielectric constant $\epsilon_h$ in $\Omega_2$ from 78.5 to 5, while the dielectric constant in $\Omega_1$ and $\Omega_3$ remained constant at 78.5. The dielectric constant of graphene ($\epsilon_G = 4$) was the same as our previous work[34]. The average ionic fluxes at the exit of permeate side were sampled and compared among those under varied potential conditions and concentration differences. The results are summarized in the Supplementary Fig. 6. All simulations were carried out with the COMSOL software package.

We further considered the effect of a possible increase in the intrinsic ion mobility when subjected to severe nanoconfinement and with an externally applied electric field on enhanced channel permeability across ${\Omega_2}^3$. The results of a $V_g = -0.2$ V were shown in the Supplementary Fig. 7. It can be seen that the variation of ion mobility can result in a higher ionic flux. In a permeate electrolyte concertation of 0.05 M, the overall flux under a $V_g = -0.2$ V became higher than that under a $V_g = 0$ V when the ion diffusivity was to increase by a factor of 10. Nevertheless, such a sharp increase in ion diffusivity required to compensate the suppression from co-ion exclusion on flux was very unlikely according to existing nanofluidics theories[35]. Furthermore, the present model also indicated that the magnitude of the diffusion flux enhancement was favourable for high feed concentrations ($\Delta n$ = 0.5 M), opposite of our experimental observations.

*MD simulation of the electrical double layers confined in a 2-nm graphene nanochannel*

MD simulation was further carried out to study in more detail the EDLs structure confined in graphene nanochannels in equilibrium. A "H" shaped graphene channel structure was constructed (Supplementary Fig. 9), and periodic boundary condition was applied making any 5.7 nm-length reservoir connected to a 5 nm-length graphene nanochannel or vice versa. The LJ parameters of ions and graphene atoms was taken from literature and the TIP4P-PPPM water model[36] was employed. Columbic interactions were calculated with a particle-particle particle-mesh (PPPM) solver. During all simulations, the temperature was held constant via a Berendsen thermostat at 300 K via the LAMMPS MD code.

Initially, 1 M KCl solution and pure water were filled respectively in reservoir and nanochannel. The Constant Charge Methods (CPM)[17] were employed to vary the charge density status of graphene atoms (green) from 0 ~ –150 mC/cm$^2$. Counter-ions were added into the reservoir to retain electroneutrality. Within the first 0.8 ns, a layer of ghost atoms (at the gate of nanochannel) blocked the entrance of ions, while allowing the exchange of water between reservoirs and the nanochannel. Once the equilibrium was reached, the ghost atoms were removed, allowing ions to diffuse freely into the nanochannel. Simultaneously, the decrease in ionic concentration in the reservoir was compensated by ion insertion. For every 10 fs, the reservoir concentration was checked and toped back up to 1 M by inserting ion pairs at the reservoir centers. When the equilibrium (> 20~30 ns) was reached, the concentration check and ion insertion were turned off. The system configuration at equilibrium for the last 7~8 ns was dumped for post-analysis.

The ion concentration in reservoirs at the last stage was measured to be 1.02 ~ 1.05 M. It should be noted that the enormous computation expense associated with simulating the electrostatically modulated ion diffusion, specifically in term of a low feed concentration (50 mM) and in a relatively long nanochannel (10 ~ 100 nm), made it impractical to carry out such dynamic ion diffusion study directly using MD.

MD simulation was also used to quantify the variation of dielectric constant when confined in a nanochannel with size of 2 nm. The electric potential away from the graphene wall surface was obtained by the integral of 1D Gauss' law. The contributions from graphene plus ions, and the water molecules were calculated separately following the definition in our previous work[17]. Supplementary Fig. 9b showed the potential profiles of $\phi_{ion}$ and $\phi_{water}$ off the channel wall and that of their combination $\phi_{net}$. The average dielectric constant of water molecules was derived from $\epsilon_d = \phi_{ion}/\phi_{net}$. The calculation of the medium dielectric constant gave a value of 10, consistent with previous theoretical calculations and experiment observation[28]. This value was used in numerical simulation cases (for both PNP and PNP/IC models).

*Effect of ion correlations on diffusion through charged graphene nanochannels*

561 It is well acknowledged that EDLs rendered an oscillating layer structure within a few
562 nanometers off the electrode/electrolyte interface. Such an oscillating structure could be
563 generally explained by the presence of short-range ion correlations that led to effects of
564 "overscreening"[24] and "charge inversion"[25, 26] at a charged electrode/electrolyte interface.
565 Given such an overscreening can result in a more concentrated co-ion layer, the incorporation
566 of an ion-correlation effect was investigated, as was its impact on ion diffusion properties
567 through a charged graphene nanochannel.
568
569 The model used was one developed recently by Bazant and colleagues[24], and named as the
570 Poisson-Nernst-Planck model with Ion Correlation (PNP/IC) that shows better descriptions
571 especially on the oscillating EDLs structure than the previous PNP model. The governing
572 equations are,

$$\epsilon_0\epsilon\nabla^2\phi(\mathbf{r}) - \epsilon_0\epsilon {l_c}^2\nabla^4\phi(\mathbf{r}) = -\rho(\mathbf{r}) = -\sum_{i=i}^{N} z_i e N_A\, n_i \quad \text{Eq.4}$$

$$\frac{\partial n_i}{\partial t} = D_i\nabla^2 n_i + e z_i \mu_i n_i \nabla\phi(\mathbf{r}) + \frac{D_i N_A a^3 n_i \nabla(n_+ + n_-)}{1 - N_A a^3 (n_+ + n_-)} \quad \text{Eq.5}$$

573 Compared with the previous modified PNP model, an extra forth order Laplace operator was
574 added for the correction for ion-ion correlation and $l_c$ for correlation length.
575
576 The channel geometry and configuration were the same as shown in the Supplementary Fig.
577 5. According to the MD simulation study, the dielectric constant in $\Omega_2$ was set at $\epsilon_d = 10$,
578 and ion size and correlation length given as $a = l_c$ = 0.66 nm for aqueous KCl solution were
579 employed. The boundary conditions in PNP/IC modeling were the same as that in the
580 previous PNP model, and the equal flux of cation and anion was maintained at the exit as a
581 result of diffusion potential. The numeric implementation of PNP/IC model in COMSOL was
582 followed by the suggestion by Liu, *et. al.*[37] and Xie, *et. al.*[38].
583
584 Such a different flux – potential relationship revealed with the PNP/IC model was attributed
585 to the increase of the co-ion (anion) concentration as a result of the strong ion-ion correlation.
586 The average concentration in $\Omega_2$ over different applied channel potential was plotted in Fig.
587 4. At a low voltage range of 0 ~ 0.1 V, the exclusion of co-ions resulted in a decrease of the

588 overall anion concentration, thus the ion diffusion flux. When the applied potential increased,
589 the cation-anion correlations dominated the first-layer counter-ion screening, resulting in an
590 increase of both counter- and co-ion concentrations, and thus an enhanced ionic flux. It was
591 also seen that lower feed reservoir concentrations corresponded to a more significant EDL
592 structure change, reflected by a larger degree of variations in both co- and counter-ion
593 concentrations for a given channel potential. In addition, the result of various channel
594 dielectric constant ($\epsilon_d$) from 78.5 to 10 in the PNP/IC model were also plotted in the
595 Supplementary Fig. 10, to show the effect of an increasing nano-confinement. Similar to the
596 claim by Bazant *et. al.*[24], with the increase of dielectric constant, the screening of solvent
597 precedes the correlations among the ions, and the PNP/IC model reduces to the general PNP
598 model with an negligible contribution from the ion-ion correlations term in Eq. 4. However
599 under severe nanoconfinement, the ion-ion correlations effect has a significant influence on
600 the distribution and dynamics of ions in the EDL.
601
602 Although the PNP/IC model appeared to successfully reproduce most of the experimental
603 observations, it could not be definitely concluded that the origin of the as-observed,
604 experimental permeability enhancement could be attributed to the anomalously strong ion-ion
605 correlations. Rather, the results presented here suggest a basic research framework upon
606 which future understanding can be built by studying the effect of ion-ion correlations on ion
607 dynamics, particularly in nanoconfined aqueous liquid systems.
608
609 **Data availability**
610 The data that support the plots within this paper and other findings of this study are available
611 from the corresponding author upon reasonable request.
612
613 **References for the Methods**

614 30. Li, D., Muller, M. B., Gilje, S., Kaner, R. B., Wallace, G. G. Processable aqueous
615 dispersions of graphene nanosheets. *Nat. Nanotechnol.* **3**, 101-105 (2008).
616
617 31. Qiu, L. et al. Controllable corrugation of chemically converted graphene sheets in
618 water and potential application for nanofiltration. *Chem. Commun.* **47**, 5810-5812
619 (2011).
620

32. Kornyshev, A. A. Double-layer in ionic liquids: paradigm change? *J. Phys. Chem. B* **111**, 5545-5557 (2007).

33. Ghoufi, A., Szymczyk, A., Renou, R., Ding, M. Calculation of local dielectric permittivity of confined liquids from spatial dipolar correlations. *EPL* **99,** 37008 (2012).

34. Daiguji, H., Yang, P., Majumdar, A. Ion transport in nanofluidic channels. *Nano Lett.* **4**, 137-142 (2003).

35. Daiguji, H. Ion transport in nanofluidic channels. *Chem. Soc. Rev.* **39**, 901-911 (2010).

36. Horn, H. W. et al. Development of an improved four-site water model for biomolecular simulations: TIP4P-Ew. *J. Chem. Phys.* **120**, 9665-9678 (2004).

37. Liu, J. L. Numerical methods for the Poisson–Fermi equation in electrolytes. *J. Comput. Phys.* **247,** 88-99 (2013).

38. Xie, D., Liu, J. L., Eisenberg, B. Nonlocal Poisson-Fermi model for ionic solvent. *Phys. Rev. E* **94,** 012114 (2016).

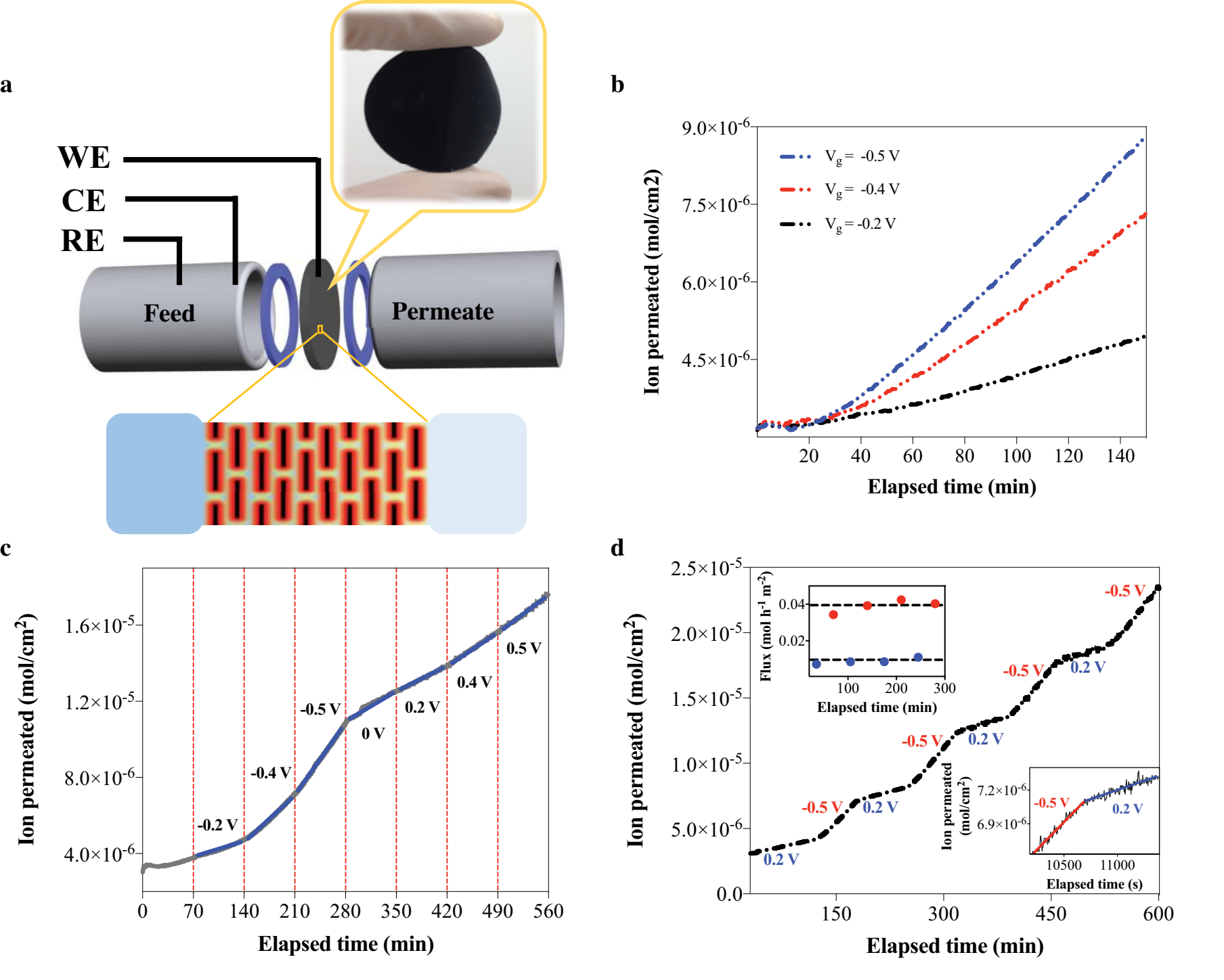
a
WE
CE
RE
Feed
Permeate
b
Ion permeated (mol/cm2)
9.0×10-6
7.5×10-6
6.0×10-6
4.5×10-6
Vg = -0.5 V
Vg = -0.4 V
Vg = -0.2 V
20
40
60
80
100
120
140
Elapsed time (min)
c
Ion permeated (mol/cm2)
1.6×10-5
1.2×10-5
8.0×10-6
4.0×10-6
-0.2 V
-0.4 V
-0.5 V
0 V
0.2 V
0.4 V
0.5 V
0
70
140
210
280
350
420
490
560
Elapsed time (min)
d
Ion permeated (mol/cm2)
2.5×10-5
2.0×10-5
1.5×10-5
1.0×10-5
5.0×10-6
0.0
Flux (mol h-1 m-2)
0.04
0.02
100
200
300
Elapsed time (min)
-0.5 V
0.2 V
Ion permeated (mol/cm2)
7.2×10-6
6.9×10-6
10500
11000
Elapsed time (s)
150
300
450
600
Elapsed time (min)

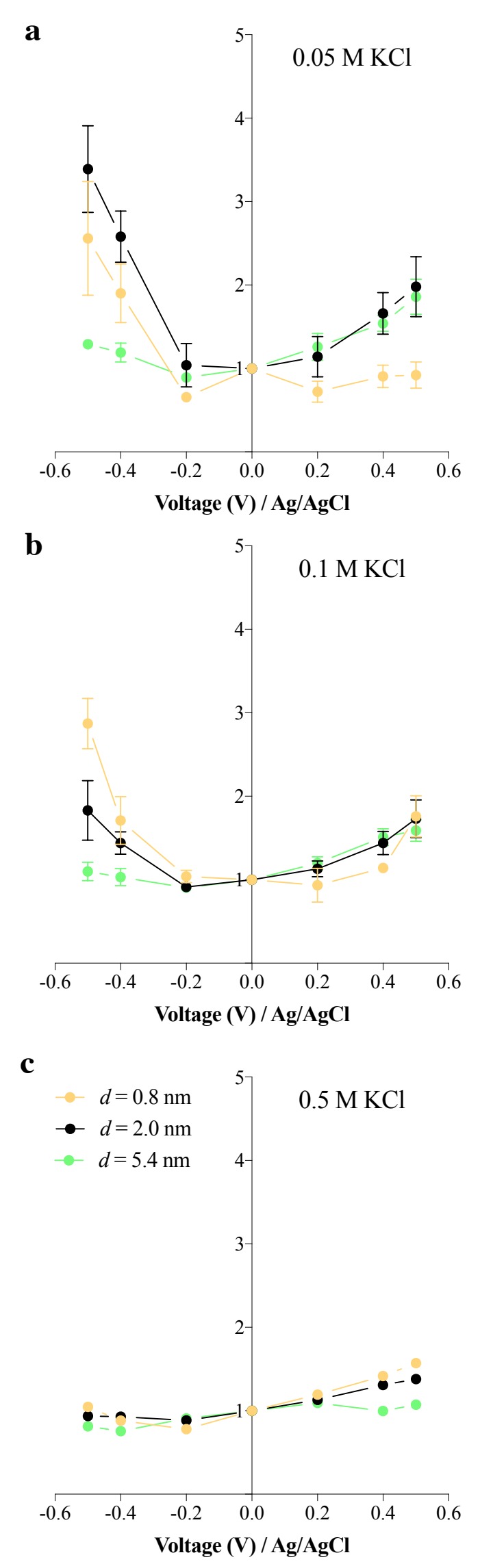
a
0.05 M KCl
5
4
3
2
1
-0.6
-0.4
-0.2
0.0
0.2
0.4
0.6
Voltage (V) / Ag/AgCl
b
0.1 M KCl
5
4
3
2
1
-0.6
-0.4
-0.2
0.0
0.2
0.4
0.6
Voltage (V) / Ag/AgCl
c
d = 0.8 nm
d = 2.0 nm
d = 5.4 nm
0.5 M KCl
5
4
3
2
1
-0.6
-0.4
-0.2
0.0
0.2
0.4
0.6
Voltage (V) / Ag/AgCl

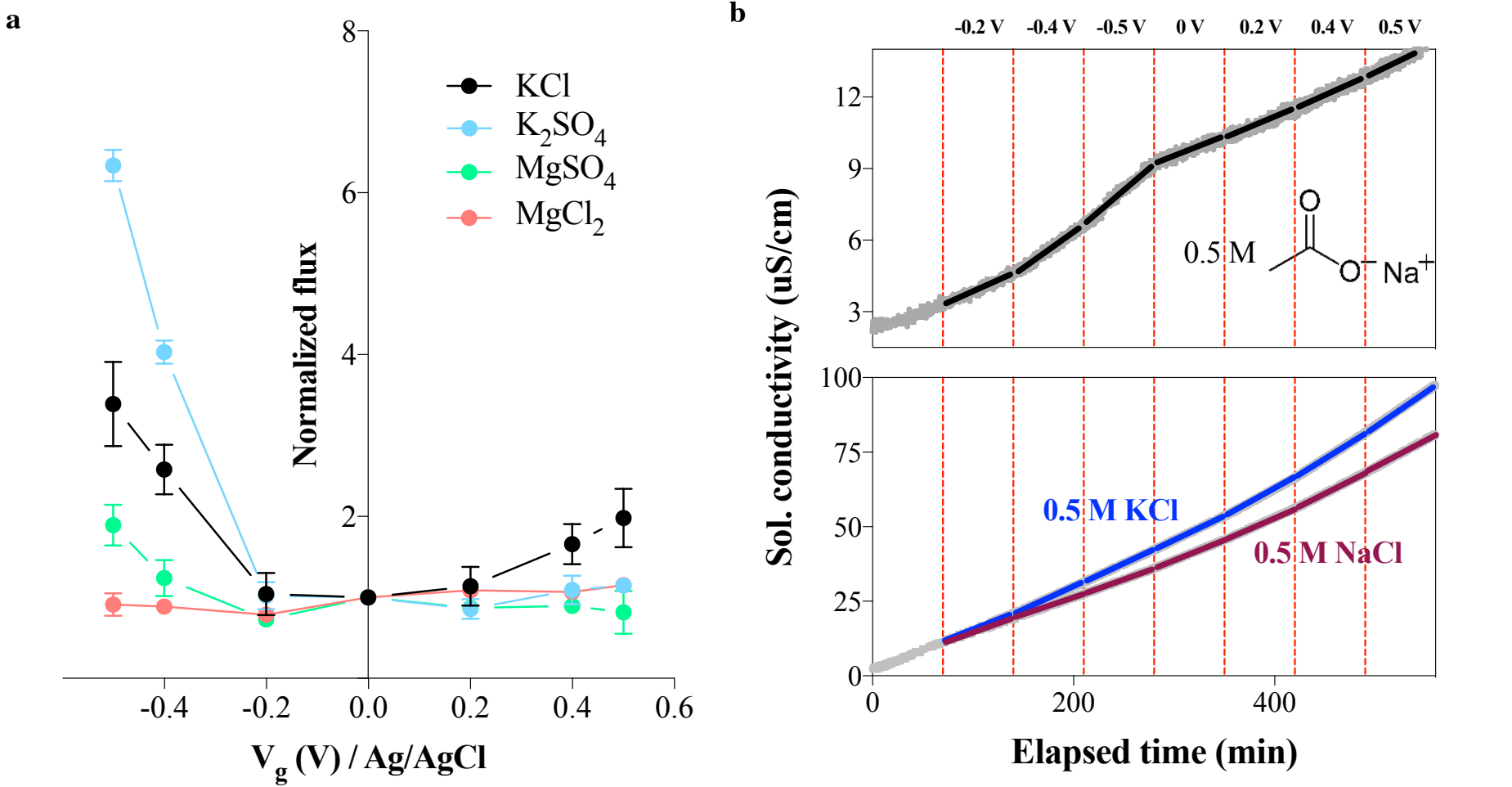
a
b
KCl
K2SO4
MgSO4
MgCl2
Normalized flux
Vg (V) / Ag/AgCl
-0.2 V
-0.4 V
-0.5 V
0 V
0.2 V
0.4 V
0.5 V
0.5 M
Na+
0.5 M KCl
0.5 M NaCl
Sol. conductivity (uS/cm)
Elapsed time (min)

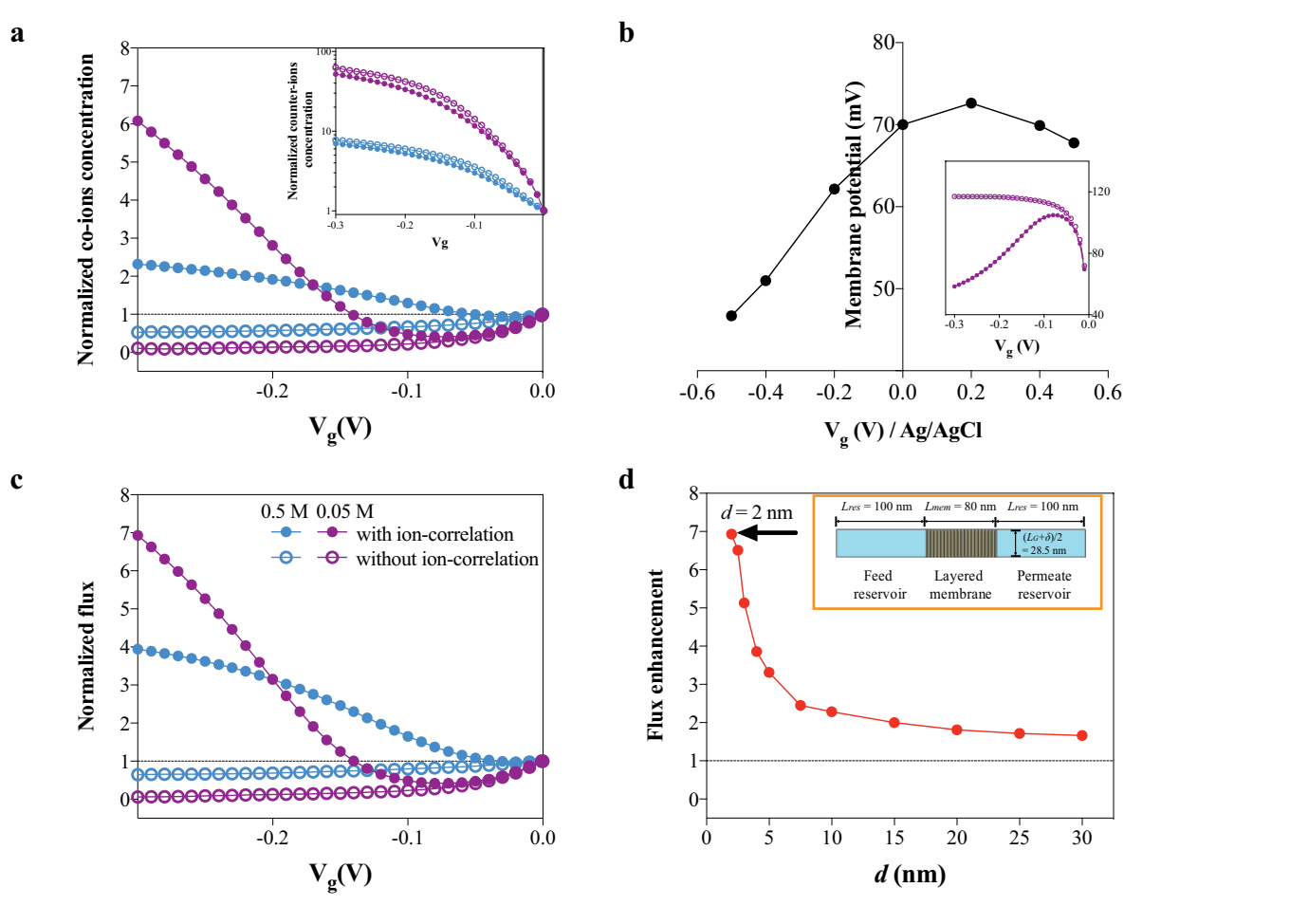
a
Normalized co-ions concentration
Normalized counter-ions concentration
Vg
Vg(V)
b
Membrane potential (mV)
Vg (V)
Vg (V) / Ag/AgCl
c
0.5 M 0.05 M
with ion-correlation
without ion-correlation
Normalized flux
Vg(V)
d
d = 2 nm
Lres = 100 nm
Lmem = 80 nm
Lres = 100 nm
(Lc+δ)/2 = 28.5 nm
Feed reservoir
Layered membrane
Permeate reservoir
Flux enhancement
d (nm)